Applied Physics A (2022) 128:483
https://doi.org/10.1007/s00339-022-05622-w

Applied Physics A
Materials Science & Processing

Synthesis of nanocubic lithium cobalt ferrite toward high-performance lithium-ion battery

Ebtesam E. Ateia[1,2] · Mahmoud A. Ateia[1] · Motaz G. Fayed[3] · Soliman. I. El-Hout[4] · Saad G. Mohamed[3] · M. M. Arman[1]

Received: 6 January 2022 / Accepted: 19 April 2022 / Published online: 12 May 2022

Abstract

The synthesis of $Li_{1.1}Co_{0.3}Fe_{2.1}O_4$ ferrite nanoparticles has been successfully fabricated by the citrate auto combustion technique. Numerous characterization techniques as X-ray Diffraction (XRD), High- Resolution Transmission Electron Microscopy (HRTEM), Field emission scanning electron microscope (FESEM), and Raman Spectroscopy are achieved. The homogeneous formation of the cubic phase is ratified through HRTEM. Five Raman-active modes A_{1g}, $3F_{2g}$, E_g. are detected for the examined samples. In addition, X-ray photoelectron spectroscopy (XPS) is carried out to identify the various ions existing in samples and their oxidation states. The investigated ferrite nanoparticles manifest large capacity (until 1150 mAh g^{-1}), stellar coulombic efficiency, and superb cycle stability (443 mAh g^{-1} after 50 cycles). Finally, the cheap and non-toxic $Li_{1.1}Co_{0.3}Fe_{2.1}O_4$ has been employed as an anode for lithium-ion batteries (LIBs), demonstrating superior electrochemical in terms of specific capacity, cycle performance, and rate capability.

Keywords Spinel ferrites · $Li_{1.1}Co_{0.3}Fe_{2.1}O_4$ · Auto-combustion technique · Lithium-ion battery

1 Introduction

The widely used electrode material for the lithium-ion battery (LIB) is graphite (anode) and $LiCoO_2$, $LiNiMnCoO_2$ and $LiFePO_4$ (cathode). Their theoretical lithium storage capacities are 372, 140 (3–4.2 V), 150 (3.5–5 V) and 170 mA h g^{-1} (2.5–4.2 V), respectively [1]. The small theoretical capacity is the main disadvantage and the demerit of the graphite-based anode [2]. Consequently, it is highly necessary to seek alternative materials that possess higher theoretical capacities. The non-toxic, low-cost high energy density (HED), with better cycling stability, are crucial demands for new electrode materials [3, 4].

Lithium ferrite is an important transition metal (TM) spinel nanoparticle with various advantages [5, 6] making it a good candidate for utilization as an electrode. It has been widely testified for various technological applications such as the components in microwave equipment and cathode materials in LIB [7, 8]. Among the numerous electrode materials, lithium cobalt oxide $LiCoO_2$ and Iron-based compounds including. $LiFeO_2$ have high theoretical capacities and are non-toxic, and environmentally friendly [9, 10].

The magnetic property of some ferrite materials can be adjusted through electrochemical studies [11, 12]. The manufacture of modulable instruments controlled by Li-ions is highly affected by the existence of magnetization and ion storage ability. During the battery cycle, the TM electrodes in LIB will experience, successions of redox reactions. Accordingly, the state of the 3d electrons, as well as the magnetization, will be varied. Therefore, the management of magnetic strength by intercalation/deintercalation of Li-ions is expectable [13, 14].

Most of the research is focused on the change of the structure during the battery cycle. However, the magnetism

✉ Ebtesam E. Ateia
drebtesam2000@yahoo.com; ebtesam@sci.cu.edu.eg

1 Physics Department, Faculty of Science, Cairo University, Giza, Egypt

2 Academy of Scientific Research and Technology (ASRT), Cairo, Egypt

3 Mining and Metallurgy Engineering Department, Tabbin Institute for Metallurgical Studies (TIMS), Tabbin, Helwan 109, Cairo 11421, Egypt

4 Nanomaterials and Nanotechnology Department, Central Metallurgical Research and Development Institute, Advanced Materials Institute, Helwan, P.O. Box: 87, Cairo 11421, Egypt

evolution through 3d transition-metal (TM) oxides didn't catch the researchers' attention. In spite of the importance of structural classification of the electrodes, the magnetic measurement appears to be an accurate, sensitive, and appropriate description technique that achieves data on the detailed atomic interaction during the intercalation/deintercalation of Li-ions. Numerous binary TM ferrites have been scrutinized for supercapacitor applications as $ZnFe_2O_4$, [15] $CoFe_2O_4$, [16] $MnFe_2O_4$, [17] and $CuFe_2O_4$, [18]. Compared to other battery systems, the LIB battery offers the highest development potential for electric and hybrid electric vehicles. This is mainly because lithium has a low electronegativity (0.98 on Pauling scale) and the lowest atomic weight (6.94 g mol^{-1}) of all metals. $Li_{1.1}Co_{0.3}Fe_{2.1}O_4$ (LiCoFeO) sample has a clear advantage in terms of cost, higher electrochemical potential, the HED and it is relatively less toxic [19].

Widespread commercial use of nanoparticles in energy devices will require more sophisticated electrode formulations and better recognition of the nature of charge storage. Consequently, this work is motivated by a need for a deeper understanding of nanoparticles for use as active material in LIBs.

In the current work, the LiCoFeO nano ferrite was prepared via the citrate auto combustion technique. The structure, morphology, oxidation states of numerous ions and the appropriateness of the investigated samples to be used as LIB electrodes were testified in detail, especially specific capacity, cycle performance, high reversible lithium storage capacity and rate capability.

2 Experimental work

2.1 Preparation of LiCoFeO

LiCoFeO was synthesized using the citrate auto combustion approach through the blending of non-stoichiometric amounts of lithium, cobalt, and iron nitrates with the estimated amount of citric acid, as stated earlier [20], with certain modifications as indicated in Fig. 1. All the chemical reagents were obtained from Sigma-Aldrich Company and used without additional treatment.

2.2 Electrode fabrication and electrochemical measurements

The electrochemical behavior of LiCoFeO ferrite nanoparticles as an anode material for LIB uses was testified utilizing the two-electrode coin cell (CR 2032). The working electrode was prepared in a glove box (I-Lab, inert, USA) under Ar atmosphere through the dissolving of 70:20:10 mass ratios of active electrode material LiCoFeO ferrite, acetylene black as the conductive material, and polyvinylidene fluoride in N-methyl-2-pyrrolidone as a binder. Thereafter, this mixture was smoothly deposited onto the copper foil (current collector) then left to dry at 95 °C overnight before pressing to 16 mm diameter. As reference and counter electrode, Li metal foil was utilized. A glassy membrane was employed as a separator. 1 M $LiPF_6$ in a 1:1 blend of dimethyl carbonate and ethylene carbonate was utilized as an electrolyte. The electrodes completed half cells were immersed in the electrolyte overnight to ensure their saturation. Cyclic voltammetry (CV) was measured from 0.01 to 3.0 V (vs. Li/Li^+) at

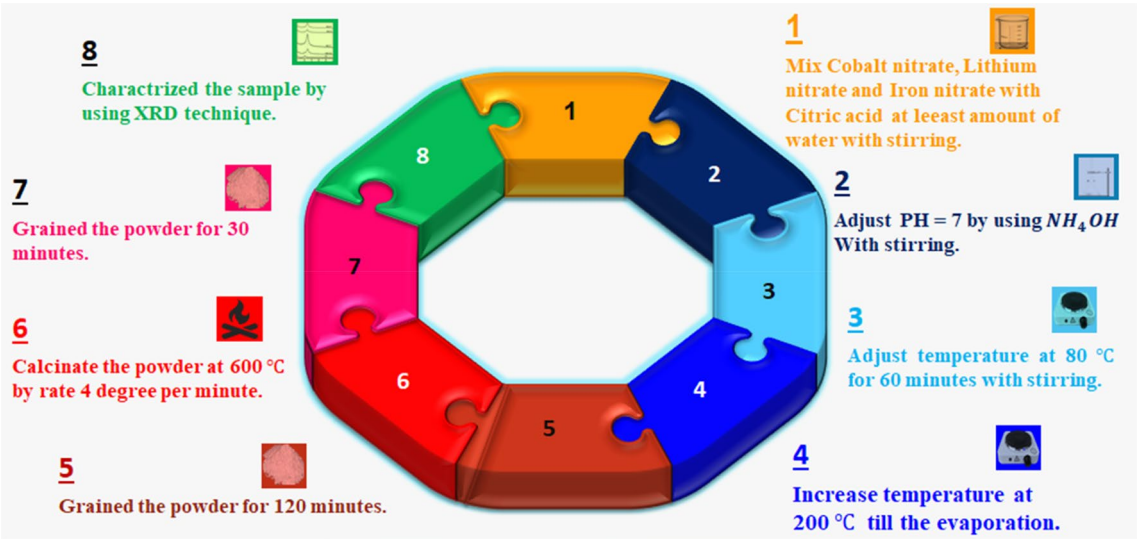

Fig. 1 Flowchart for the preparation technique of LiCoFeO

a scan rate of 0.25 mV s^{-1} using the electrochemical work station (OrigaFlex-OGF01A, OrigaLys ElectroChem SAS, France). At an open circuit voltage, electrochemical impedance spectroscopy (EIS) was performed at frequency ranging from 100 kHz to 100 MHz. A NEWARE BTS-4000 battery testing equipment was used to perform the galvanostatic charge–discharge (GCD) tests at numerous current densities.

2.3 Characterization tools

The X-ray diffractometer (Xpert PRO MPD) was used to analyze the XRD patterns of ferrite nanoparticles using CuKα radiation. High-Resolution Transmission Electron Microscopy (HRTEM) was operated to investigate the morphology and size distribution of the as-prepared ferrites. The morphology of the nanoparticles was investigated using Field Emission Scanning Electron Microscope (FESEM, model Quanta 250). The energy-dispersive X-ray analysis (EDAX) and the elemental mapping were carried out through Scanning Electron Microscope (Quanta 250 FEG) linked with EDAX system. To investigate the oxidation states of various elements in the as-prepared ferrites, X-ray photoelectron spectroscopy (XPS) analysis was performed via K-ALPHA (Thermo Fisher Scientific, USA).

3 Results and discussion

3.1 Structural analyses

3.1.1 XRD analysis

Figure 2a demonstrates the XRD chart of the LiCoFeO sample. This chart is recorded at room temperature, and all the diffraction lines are indexed for the cubic spinel phase with space group (Fd-3 m). The crystallite size (D_{XRD}) of the sample is detected according to the Williamson–Hall equations as mentioned in the previous work [20]. The obtained data assure that the sample is prepared in nano scale with crystallite size 30 nm. The XRD data is compared with JCPDS card 04-022-8066 [20].

3.1.2 Raman spectra

Figure 2b shows the Raman spectra for LiCoFeO nanoparticles. In general, the cubic-inverse spinel structure belonging to the symmetry O_h^7 with a space group (Fd3m). It has 16 cations in octahedral sites, 8 cations in tetrahedral sites, and 32 oxygen anions [21]. White et al. [22, 23] predict the following vibrational normal modes according to the group theory as given as:

$$A_{1g}(\mathrm{R}) + E_g(\mathrm{R}) + F_{1g} + 3F_{2g}(\mathrm{R}) + 2A_{2u} + 2E_u + 4F_{1u}(\mathrm{IR}) + 2F_{2u} \quad (1)$$

where the (R) and (IR) identify Raman-active and infrared-active vibrational species, respectively, and the rest of the modes are silent modes.

There are five Raman-active modes [24] that should be observed for the cubic spinel phase as shown in Equation:

$$A_{1g} + E_g + 3F_{2g} \quad (2)$$

Here A, E, and F signify one, two, and three-dimensional representations, and g signifies the symmetry of the center of inversion. The three Raman-active F_{2g} modes are labeled $F_{2g}(1)$, $F_{2g}(2)$, and $F_{2g}(3)$, where $F_{2g}(1)$ is the lowest frequency F_{2g} mode and $F_{2g}(3)$ is the highest frequency mode of this vibrational species.

As shown from the figure, three various spectral intervals can be noticed in the region 100–800 cm^{-1} for LiCoFeO as follows (i) 600–800 cm^{-1} is the region of A_{1g} modes; (ii) 410–550 cm^{-1} is the region of $F_{2g}(3)$ modes, and (iii)

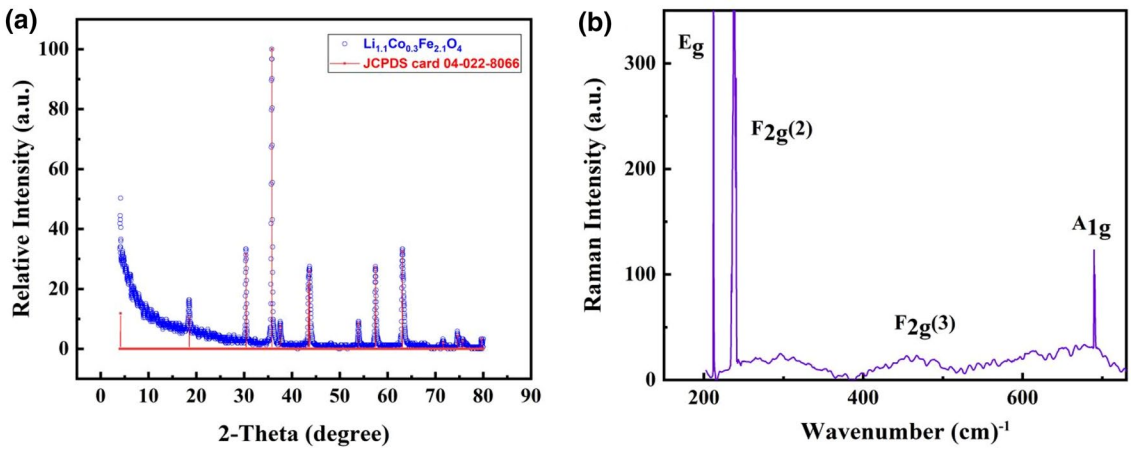

Fig. 2 **a** XRD diffraction pattern and **b** Raman spectra for Li1.1Co0.3Fe2.1O4

260–380 cm^{-1} is the region of $F_{2g}(2)$ modes. Eg and $F_{2g}(1)$ may be observed at a lower frequency. The highest-frequency A_{1g} mode is assigned to the symmetric stretching of Fe^{3+}–O at the tetrahedral (A) site within the spinel lattice [25]. All the other low-frequency modes are attributed to vibrations inside the octahedral sites (BO_6) [26].

Besides the highest-frequency, Raman-active $F_{2g}(3)$ mode is alternatively attributed to the antisymmetric bending of the tetrahedral unit [27] or the asymmetric bending motion of the oxygens bonded to the tetrahedral cations [28]. A vibrational frequency side is dependent on both the bond strength (degree of covalence and bond length affect the bond strength) and the reduced mass of the vibrational species.

The $F_{2g}(2)$ mode is due to the opposite motion of cation and oxygen along one direction of the lattice [29].The E_g mode is assigned to the symmetric bending motion of the oxygen anions with respect to ferric cations at the tetrahedral (A) site in agreement with other researchers [30].

3.1.3 Microstructural features

Figure 3a–c illustrates the HRTEM for the LiCoFeO sample with the selected area electron diffraction patterns (SAED) and the size distribution histogram.

Usually, the morphology and electrochemical performance of the spinel ferrites are susceptible to the fabrication process. The shape of the LiCoFeO nanoparticle is roughly spherical and highly agglomerated due to the magnetic nature of the cobalt. The SAED approves a highly crystallinity of the sample [31]. The mean size can be detected from Fig. 3c. It is equal to 70 nm, which is proportionate with a large surface area of the sample.

3.1.4 Field emission scanning electron microscope (FESEM)

The morphology of the sample is studied using a Field Emission Scanning Electron Microscope (FESEM) as demonstrated in (Fig. 4a–b). The nano size is ratified from the images. The grains have a rocky-like shape with porous nature. The presence of pores in the investigated sample as a result of escaping of gases during the preparation technique [32]. The morphological features recommend the use of LiCoFeO in water treatment, gas sensors and LIBs.

3.1.5 Energy-dispersive X-ray spectroscopy (EDAX) and mapping analyses

Figure 5a EDAX analysis for the LiCoFeO sample. EDAX analysis confirms the presence of elements Fe, Co, and O. While the Li element cannot be detected due to its low atomic number [33].The dispersive X-Ray spectroscope for the present objective does not have a sensing nature to reveal the energy released by a very small lithium-ion, which has a K shell for transition for auger electrons. The EDAX data detects that the sample is prepared without any impurity. The inset table gives a quantitative estimation of elements attained directly from the spectrum through its weight and atomic percentages. Figure 5b illustrates the elemental mapping of the $LiCoFeO_4$ sample. The elements cobalt, iron, and oxygen are present in the homogenous distribution

3.1.6 X-ray photoelectron spectroscopy (XPS)

The binding energy of numerous atoms is related to the chemical state of the atom and the molecular environment. The XPS technique denoted the elemental composition, the oxidation state of numerous cations, and the state in the synthesized sample. Figure 6 describes the taken XPS spectra for the LiCoFeO nanoparticles. The main peak, $Fe2p_{3/2}$, with

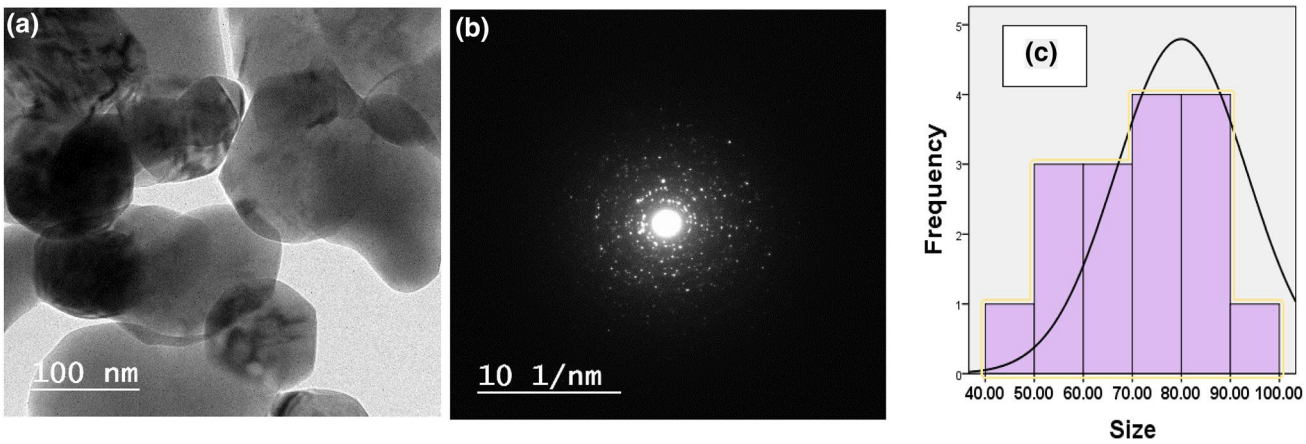

Fig. 3 **a** HRTEM for the LiCoFeO, **b** the selected area electron diffraction patterns (SAED) and, **c** histogram represents the size distribution

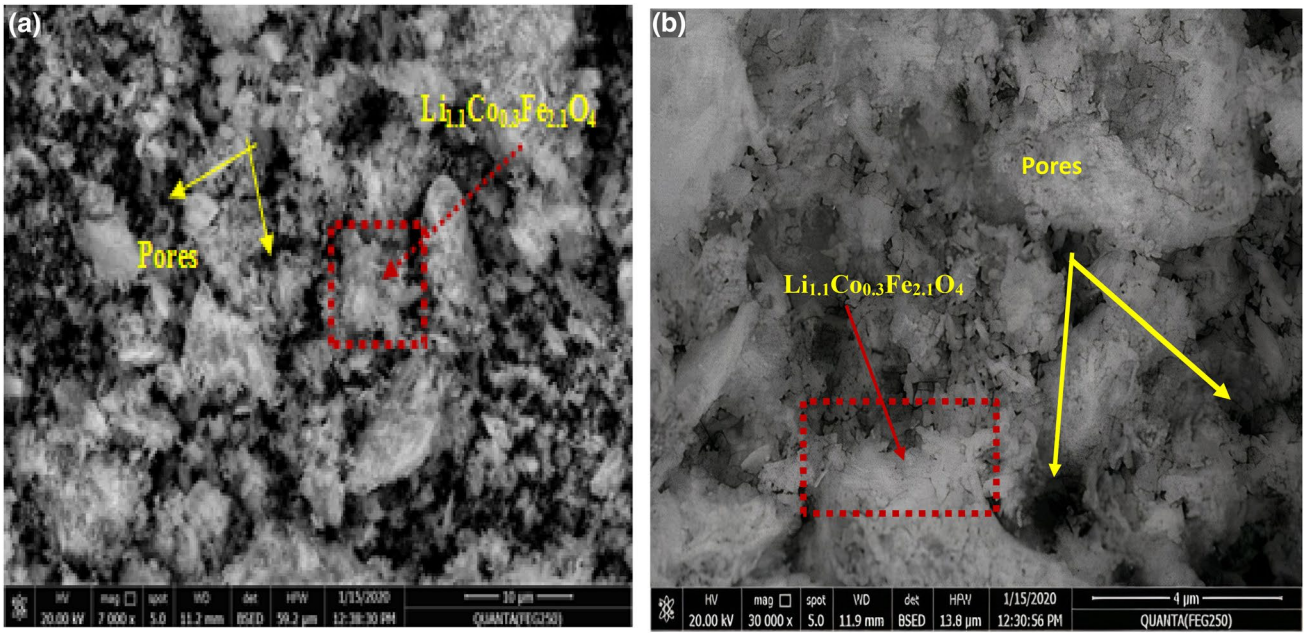

Fig. 4 **a**–**b** FESEM for the LiCoFeO

a satellite peak at 718 eV, is fitted into two signals positioned at 710 and 713 eV, signifying the presence of Fe in two different lattice sites. The binding energies of Fe^{3+} ions in octahedral sites (B) and tetrahedral sites (A) are 710 eV and 713 eV, respectively, as shown in Fig. 6b. According to the integrated intensity of the fitted doublets, the distribution of Fe^{3+} ions for both samples is obtained to be about 70% in octahedral sites and about 30% in tetrahedral sites.

The Li 1 s contribution from the active LiCoFeO is present as a weak component at ~66 eV (Fig. 6c) the weak Li signal relative to the Fe and Co signals is partly due to the difference in the photoionization cross sections for Li 1 s compared to Fe and Co.

In Fig. 6d, the Co $2p_{3/2}$ XPS spectra are well fitted into three peaks situated on 780, 783, and 785 eV. The binding energies at 779.8 and 781.9 eV are assigned to Co^{3+} in B sites and Co^{2+} in A site, respectively. The signal at 785.9 eV can be ascribed to the satellite peak of Co $2p_{3/2}$ main line [34].

The O 1 s XPS signals shown in Fig. 6e are divided into three peaks at 528.5, 531, and 532 eV. The contribution of the crystal lattice oxygen is signified by the main peak at 528.5 eV. However, the exact assignment of the higher binding energy peaks is rather complex and controversial as numerous issues like contaminants, impurities, surface defects, or chemisorbed oxygen species. Finally, the existence of LiCoFeO in the sample can be seen from the XPS spectrum, which further designates that the sample has been successfully synthesized.

3.2 Electrochemical performance

The performance of $Li_{1.1}Co_{0.3}Fe_{2.1}O_4$ powder as an electrode material for LIBs is characterized electrochemically. Figure 7 shows the CV curves for the first five cycles between 0.01 and 3.0 V (vs. Li/Li^+) at a scan rate of 0.25 mV s^{-1}. During the initial discharge process, the reduction peak at 0.52 V (vs. Li/Li^+) can be linked to a reduction reaction of Fe^{3+} and Co^{2+} with Li and the formation of Li_2O [35, 36]. The oxidation processes of metallic Fe and Co are responsible for the broad anodic peak among all [37].

Further, a broad peak is observed in the anodic polarization process at around 1.05 V (vs. Li/Li^+), which matched the oxidation of Fe^0 to Fe^{2+} and then to Fe^{3+} [37]. The CV curves for the $Li_{1.1}Co_{0.3}Fe_{2.1}O_4$ electrode are highly stable after the second cycle, showing improved steadiness through the lithiation and de lithiation operations.

The corresponding charge–discharge patterns of the LiCoFeO electrode in the voltage window of 3–0.01 V (vs. Li/Li^+) (from 1st cycle to 100th cycle is shown in Fig. 8a at a current density of 100 mA g^{-1}. A lengthy plateau emerges at around 0.85 V (vs. Li/Li^+) during the initial discharge cycle, suggesting a reduction of Fe^{3+} and Co^{2+} to Fe^0 and Co^0 as well as the formation of Li_2O, respectively [38, 39]. The electrode has an initial charge/discharge specific capacity of 770/1300 mAh g^{-1}, equating to a 59.2% initial coulombic efficiency. The coulombic efficiency reaches 98.77% after 100 cycles, suggesting that the LiCoFeO is more stable due to the creation of solid electrolyte interphase (SEI) layers on the electrode surface and hence can successfully handle

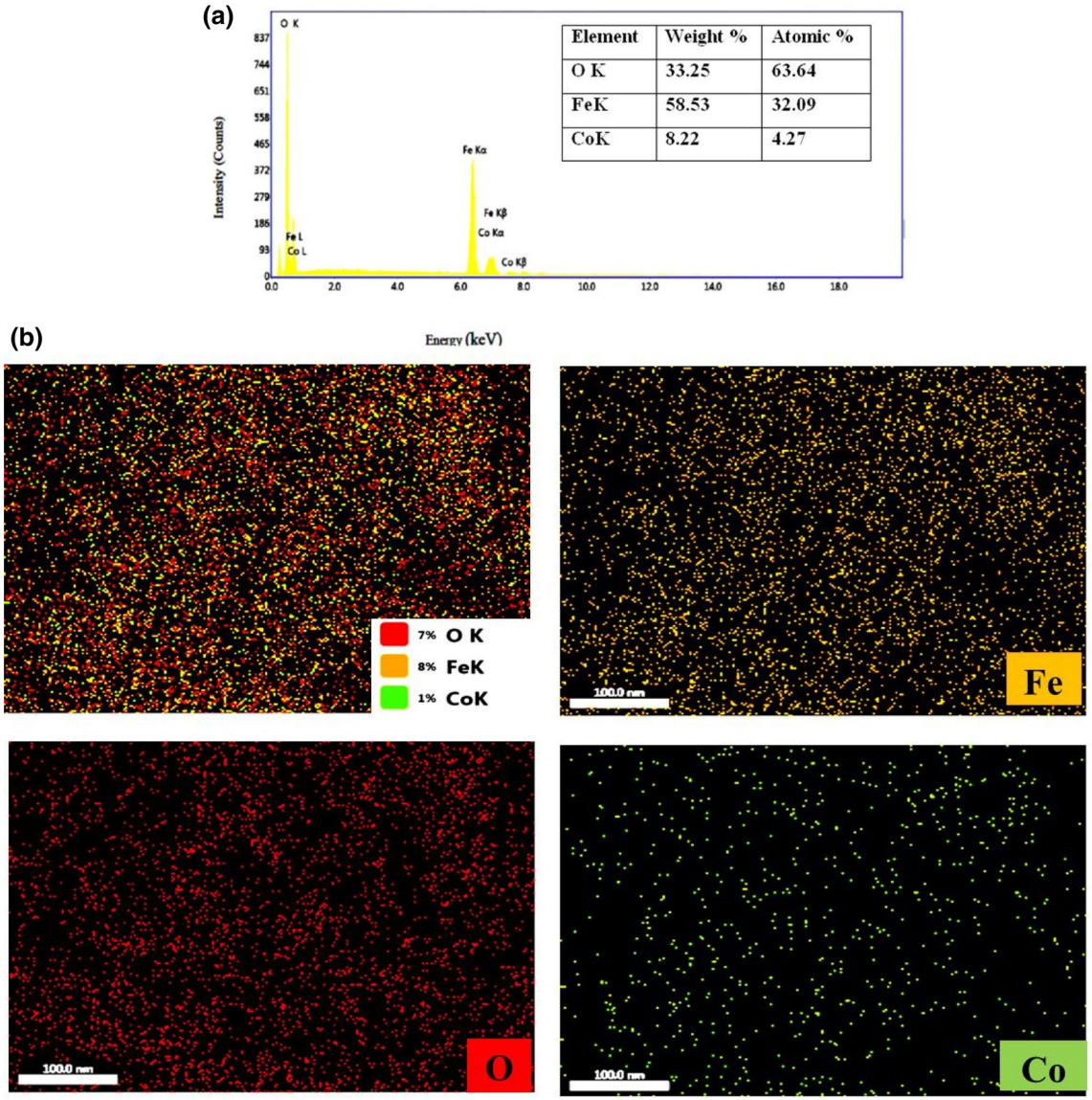

Fig. 5 **a** EDAX spectrum and **b** The elemental mapping of the $Li_{1.1}Co_{0.3}Fe_{2.1}O_4$ sample

volume variations [40, 41] as presented in Fig. 8b. The LiCoFeO electrode initial capacity loss was 40.8%, which may be due to the irreversible surface reactions, such as (i) Lithium ions capture inside the lattice, (ii) Li^+ ions intercalation/deintercalation into/out of an acetylene carbon black conductor iii) solid electrolyte interphase (lithium alkyl carbonates) formed on the electrode [42].

Another significant characteristic of high-performance LIBs is their rate capabilities. The rate capability performance of the LiCoFeO electrode is investigated at varied current densities of 100, 200, 500, 800, 1000, and 2000 mA g^{-1}, as shown in Fig. 8c. After 42 cycles, the LiCoFeO electrode reversible discharge specific capacity is 1150, 390, 265, 170, 140 and 110 mAh g^{-1}, at current densities of 100, 200, 500, 800, 1000 and 2000 mA g^{-1}, sequentially. When 50 cycles, the LiCoFeO electrode exhibits a high rate performance with a specific capacity of 443 mAh g^{-1} after the current density progressively recovered to 100 mA g^{-1}. The improvement in rate capability might be attributed to the presence of the highly conducting Li ions and the small size of LiCoFeO ferrite nanoparticles which facilitates the Li-ions mobility [35]. Moreover, the cubic 3D structure of LiCoFeO is favorable for the preferable moistening of the electrode material via the electrolyte, thus facilitating the lithiation and delithiation across the electrolyte/electrolyte interface [36].

The performance of the electrode materials is examined through EIS by elucidation of the physicochemical

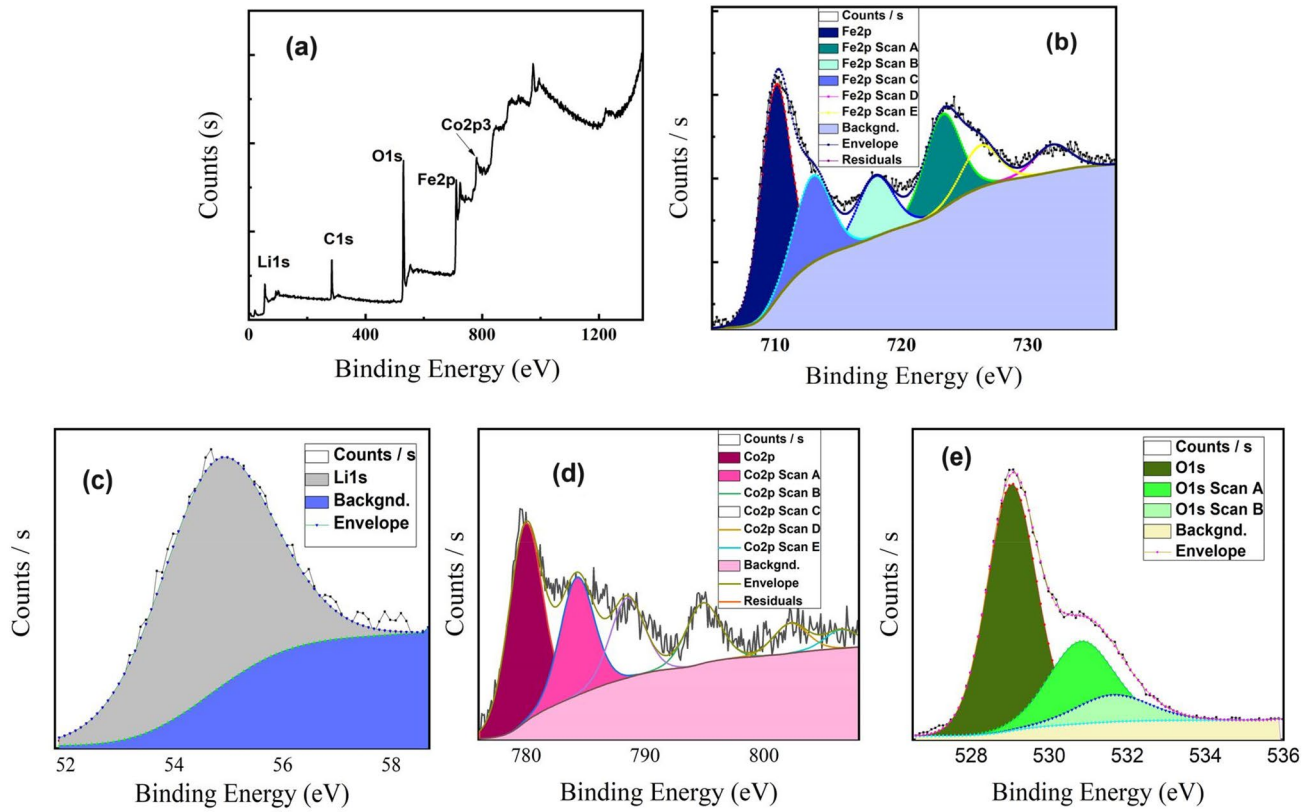

Fig. 6 XPS spectra of the LiFeCoO sample **a** Survey scan, **b** Fe2p, **c** Li1s, **d** Co2p, and **e** O1s spectra

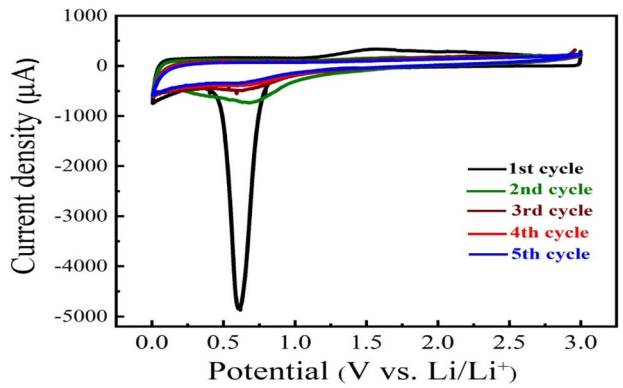

Fig. 7 Cyclic voltammogram of $Li_{1.1}Co_{0.3}Fe_{2.1}O_4$ electrode

processes. Figure 8d shows the Nyquist plot, revealing that the electrodes have two different components. The equivalent circuit includes constant phase elements (*CPE*) of double-layer capacitance, charge/transfer resistance (R_{ct}), electrolyte resistance (R_1), and Warburg impedance (W_o). The charge transport impedance at the electrode/electrolyte contact is responsible for the semicircular in the high-frequency region. The straight line (Warburg tail) is ascribed to Li^+ prevalence in the active electrode material in the low-frequency region. Before and after 100 cycles, the cells are exposed to an EIS examination, as revealed in Fig. 8d. The charge-transfer resistance (R_{ct}) after 100 cycles looks constant (changed from 114.6 to 115.2 Ω) because the contact between the electrolyte and the electrode is continually stimulated through the cycles in the high-frequency area [43].

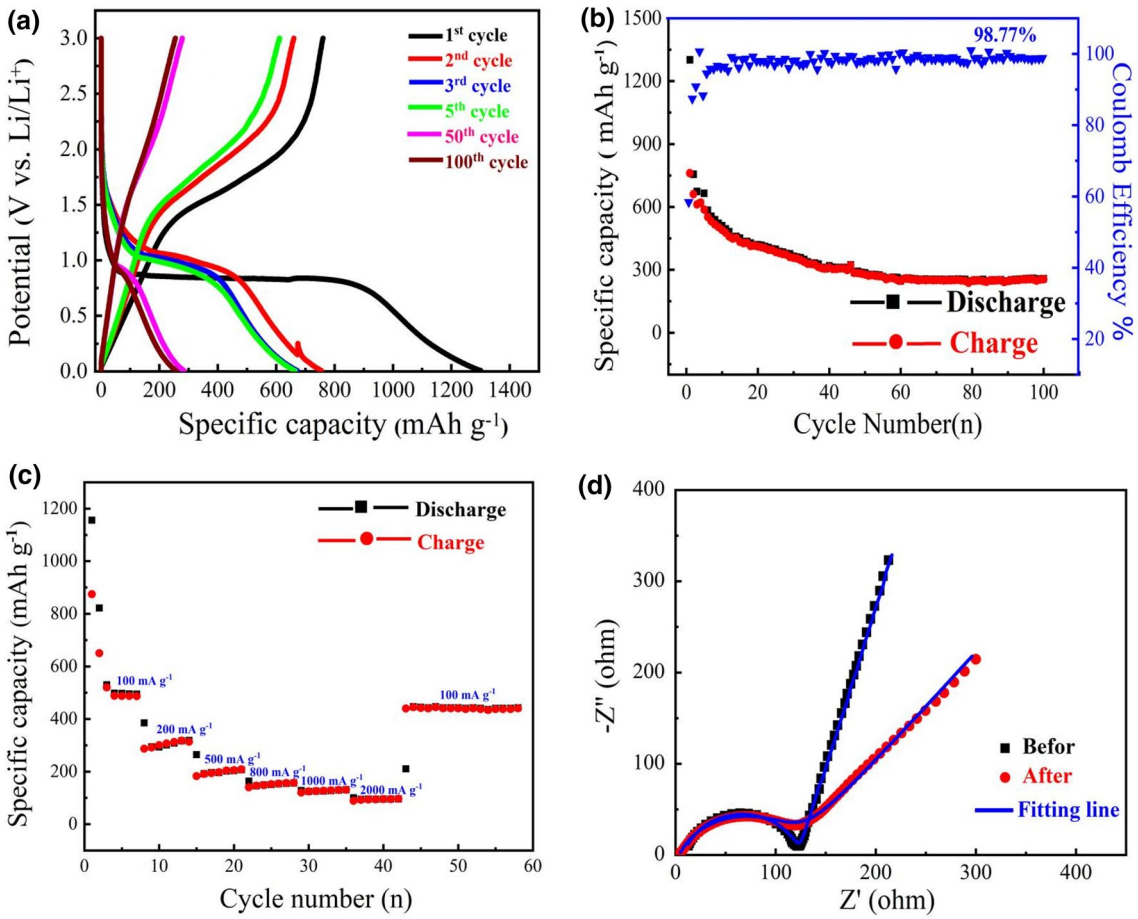

Fig. 8 **a** Charge/discharge profiles at a current density of 100 mA g^{-1}, **b** Cycling stability at a current density 100 mA g^{-1}, **c** The rate capability, and **d** EIS plot of the $Li_{1.1}Co_{0.3}Fe_{2.1}O_4$ electrode

4 Conclusion

The citrate auto combustion technique has been used to fabricate novel LiCoFeO nanoparticles with a size of ≅ 70 nm. XPS measurements support the existence of Co and Fe ions as (Co^{3+}, Fe^{3+}), and (Co^{2+}, Fe^{2+}) in octahedral and tetrahedral, respectively. The five Raman-active modes are detected for LiCoFeO with the cubic spinel structure. The electrochemical measurements show that the investigated nanoparticles as electrodes exhibit an excellent high capacity in the initial discharge, a high reversible capacity, and good cycle stability. Additionally, at 58 cycles, the LiCoFeO electrode exhibits a high-rate performance with a specific capacity of 443 mA h g^{-1}. The EIS parameters of the LiCoFeO electrode after one and 100 cycles are almost the same.

Acknowledgements This paper is supported financially by the Academy of Scientific Research and Technology (ASRT), Egypt, under initiatives of Science Up Faculty of Science (Grant No. 6643)

Funding Open access funding provided by The Science, Technology & Innovation Funding Authority (STDF) in cooperation with The Egyptian Knowledge Bank (EKB).

Declarations

Conflict of interest The authors declare that they have no conflict of interest.

References

1. Y.H. Hu, X. Li, D. Geng, M. Cai, R. Li, X. Sun, Influence of paper thickness on the electrochemical performances of graphene papers as an anode for lithium ion batteries. Electrochim. Acta **91**, 227–233 (2013)
2. A. Manthiram, Materials challenges and opportunities of lithium ion batteries. J. Phys. Chem. Lett. **2**, 176 (2011). https://doi.org/10.1021/jz1015422
3. R. Marom, S.F. Amalraj, N. Leifer, D. Jacob, D. Aurbach, A review of advanced and practical lithium battery materials. J. Mater. Chem. **21**, 9938 (2011). https://doi.org/10.1039/C0JM04225K
4. V. Etacheri, R. Marom, R. Elazari, G. Salitra, D. Aurbach, Challenges in the development of advanced Li-ion batteries: a review. Energy. Env. Sci. **4**, 3243 (2011). https://doi.org/10.1039/C1EE01598B
5. S.E. Shirsath, R.H. Kadam, A.S. Gaikwad, A. Ghasemi, A. Morisako, Effect of sintering temperature and the particle size on the structural and magnetic properties of nanocrystalline Li0.5Fe2.5O4. J. Magn. Magn. Mater. **323**, 3104 (2011). https://doi.org/10.1016/j.jmmm.2011.06.065
6. D. Zhang, W. Shu, S. Li, X. Zhang, A. Ying, Z. Tong, Fabrication and characterization of Li0.5Fe2.5O4 octahedrons via a TEA-assisted route. J. Mater. Sci. **43**(17), 5948 (2008). https://doi.org/10.1007/s10853-008-2856-y
7. Y.-P. Fu, C.-H. Lin, C.-W. Liu, Y.-D. Yao, Microwave-induced combustion synthesis of Li0.5Fe2.5O4 powder and their characterization. J. Alloys Compd. **395**, 247 (2005). https://doi.org/10.1016/j.jallcom.2004.11.049
8. M. George, S. S. Nair, A. M. John, P. A. Joy, M. R. Anantharaman. Structural, magnetic and electrical properties of the sol-gel prepared Li0.5Fe2.5O4 fine particles. J. Phys. D: Appl. Phys. **39**, 900, (2006) https://iopscience.iop.org/issue/0022-3727/39/5
9. Y.C. Dong, Y.S. Chui, R.G. Ma, C.W. Cao, H. Cheng, Y.Y. Li, J.A. Zapien, One-pot scalable synthesis of Cu-CuFe2O4/graphene composites as anode materials for lithium-ion batteries with enhanced lithium storage properties. J. Mater. Chem. A **2**, 13892–13897 (2014). https://doi.org/10.1039/C4TA02203C
10. M.M. Rahman, J.-Z. Wang, M.F. Hassan, S. Chou, Z. Chen, H.K. Liu, Nanocrystalline porous α-LiFeO2–C composite—an environmentally friendly cathode for the lithium-ion battery†. Energy. Env. Sci. **4**, 952 (2011). https://doi.org/10.1039/C0EE00527D
11. Y. Mizuno et al., Precise electrochemical control of ferromagnetism in a cyanide-bridged bimetallic coordination polymer. Inorg. Chem. **51**, 10311–6 (2012). https://doi.org/10.1021/ic301361h
12. M. Okubo et al., Ion-induced transformation of magnetism in a bimetallic CuFe prussian blue analogue. Angew. Chem. Int. Ed. Engl. **50**, 6269–6273 (2011). https://doi.org/10.1002/ange.201102048
13. J. Zhang, R.D. Averitt, Dynamics and control in complex transition metal oxides. Annu. Rev. Mater. Res. **44**, 19–43 (2014). https://doi.org/10.1146/annurev-matsci-070813-113258
14. C. Yun et al., Fabrication of FeOx thin films and the modulation of transport and magnetic properties by resistance switching in Au/α-Fe2O3/Pt heterostructure. J. Appl. Phys. **115**, 17C306 (2014). https://doi.org/10.1063/1.4868077
15. L. Zhuang, C. Jianghang, X. Zhigang, Z. Jingjing, F. Meiqiang, W. Denghu, Y. Hua, Self-assembled ZnFe2O4 hollow spheres/GO hybrid anode with excellent electrochemical performance for lithium-ion batteries. J. Mater. Sci: Mater. Electronics. **31**, 1126–1134 (2020)
16. L.I.U. Jiaming et al., Combustion synthesized macroporous structure MFe2O4 (M= Zn, Co) as anode materials with excellent electrochemical performance for lithium ion batteries. J. Alloys. Compd. **699**, 401–407 (2017). https://doi.org/10.1016/j.jallcom.2016.12.225
17. W. Guodong, W. Lin, W. Dong, C. Yanxue, T. Yufeng, Y. Shishen, M. Liangmo, J. Jun, 3Reversible control of the magnetization of spinel ferrites based electrodes by lithium-ion migration. Sci. Rep. **7**, 12554 (2017)
18. L. Luo, R.R. Cui, H. Qiao, K. Chen, Y.Q. Fei, D.W. Li, Z.Y. Pang, K. Liu, Q.F. Wei, High lithium electroactivity of electrospun $CuFe_2O_4$ nanofibers as anode material for lithium-ion batteries. Electrochim. Acta **144**, 85–91 (2014)
19. C. Iclodean, B. Varga, N. Burnete, D. Cimerdean, B. Jurchiş, Comparison of different battery types for electric vehicles. IOP Conf. Ser: Mater. Sci. Eng. **252**, 012058 (2017)
20. E.E. Ateia, Assessing of channel structure and magnetic properties on heavy metal ions removal from water. J. Mater. Sci. Mater. Electron. (2021). https://doi.org/10.1007/s10854-021-07008-9
21. Z. Wang, D. Schiferl, Y. Zhao, H.S.C. O'Neill, High pressure Raman spectroscopy of spineltype ferrite ZnFe2O4. J. Phys. Chem. Solids **64**, 25172523 (2003). https://doi.org/10.1016/j.jpcs.2003.08.005
22. W.B. White, B.A. DeAngelis, Interpretation of the vibrational spectra of spinels. Spectrochim. Acta **23A**, 985–995 (1967). https://doi.org/10.1016/0584-8539(67)80023-0
23. H. Cynn, S.K. Sharma, T.F. Cooney, M. Nicol, High-temperature Raman investigation of order-disorder behavior in the $MgAl_2O_4$ spinel. Phys. Rev. B. **45**(1), 500–502 (1992). https://doi.org/10.1103/PhysRevB.45.500
24. S. Thota, S.C. Kashyap, S.K. Sharma, V.R. Reddy, Micro Raman, Mssbauer and magnetic studies of manganese substituted zinc ferrite nanoparticles: role of Mn. J. Phys. Chem. Solids **91**, 136–144 (2016). https://doi.org/10.1016/j.jpcs.2015.12.013
25. C.M. Julien, M. Massot, Lattice vibrations of materials for lithium rechargeable batteries I lithium manganese oxide spinel. Mater. Sci. Eng. B. **97**, 217–230 (2003). https://doi.org/10.1016/S0921-5107(02)00582-2
26. P. Bruesch, F. D'Ambrogio, Lattice dynamics and magnetic ordering in the chalcogenide spinels CdCr2S4 and CdCr2Se4. Phys. Status Solidi B **50**, 513–526 (1972). https://doi.org/10.1002/pssb.2220500212
27. M.P. O'Horo, A.L. Frisillo, W.B. White, Lattice vibrations of MgAl2O4 spinel. J. Phys. Chem. Solids. **4**, 23–28 (1973). https://doi.org/10.1016/0022-3697(73)90058-9
28. G.A. Sawatzky, F.V.A.N. DER Woude, A.H. Morrish, Cation distributions in octahedral and tetrahedral sites of the ferrimagnetic Spinel CoFe2O4. J. Appl. Phys. **39**, 1204–1205 (1968). https://doi.org/10.1063/1.1656224
29. G.M. Argentina, P.D. Baba, Microwave lithium ferrites: an overview. IEEE Trans. Microw. Theory. Tech. **22**, 652–658 (1974). https://doi.org/10.1109/TMTT.1974.1128308
30. H.M. Widatallah, C. Johnson, F.J. Berry, A.M. Gismelseed, E. Jartych, J.F. Marco, F.S. Gard, M. Pekala, Synthesis and cation distribution of copper-substituted spinel-related lithium ferrite. J. Phys. Chem. Solids **67**, 1817–1822 (2006). https://doi.org/10.1016/j.jpcs.2006.04.003
31. S. Meena et al., Impact of temperature-induced oxygen vacancies in polyhedron MnFe2O4 nanoparticles: as excellent electrochemical sensor, supercapacitor and active photocatalyst. Ceram. Int. **47**, 14723–14740 (2021). https://doi.org/10.1016/j.ceramint.2020.12.217
32. M.M. Arman, Synthesis, characterization, magnetic properties, and applications of $La_{0.85}Ce_{0.15}FeO_3$ perovskite in heavy metal Pb2+ removal. J. Supercond. Nov. Magn. (2022). https://doi.org/10.1007/s10948-022-06168-x

33. L. Bernard, A. Leemann, Assessing the potential of ToF-SIMS as a complementary approach to investigate cement-based materials—applications related to alkali–silica reaction. Cem. Concr. Res. **68**, 156165 (2015). https://doi.org/10.1016/j.cemconres.2014.11.008
34. E.E. Ateia, A.T. Mohamed, Core–shell nanoarchitectonics of $CoFe_2O_4$ encapsulated $La_2Fe_2O_6$ nanoparticles for their use in various applications. J. Inorg Organomet. Polym. Mater. **32**, 1389–1399 (2022)
35. S. Liu, J. Xie, C. Fang, G. Cao, T. Zhu, X. Zhao, Self-assembly of a $CoFe_2O_4$/graphene sandwich by a controllable and general route: towards a high-performance anode for Li-ion batteries. J. Mater. Chem. **22**, 19738–19743 (2012). https://doi.org/10.1039/C2JM34019D
36. W. Qi, P. Li, Wu. Ying, H. Zeng, L. Hou, C. Kuang, P. Yao, S. Zhou, Facile synthesis of CoFe2O4 nanoparticles anchored on graphene sheets for enhanced performance of lithium ion battery. Progress. Nat. Sci: Mater. Int. **26**(5), 498–502 (2016). https://doi.org/10.1016/j.pnsc.2016.09.001
37. H. Zeng, T. Tao, Y. Wu, W. Qi, C. Kuang, S. Zhou, Y. Chen, Lithium ferrite (Li0.5Fe2.5O4) nanoparticles as anodes for lithium ion batteries. RSC. Adv. **4**, 23145 (2014). https://doi.org/10.1039/C4RA02957G
38. B. Wang, G. Wang, Z. Lv, H. Wang, In situ synthesis of hierarchical CoFe2O4 nanoclusters/graphene aerogels and their high performance for lithium-ion batteries. Phys. Chem. Chem. Phys. **17**, 27109–27117 (2015). https://doi.org/10.1039/C5CP04628A
39. H. Yang, K. Zhang, Y. Wang, C. Yan, S. Lin, CoFe2O4 derived-from bi-metal organic frameworks wrapped with graphene nanosheets as advanced anode for high-performance lithium ion batteries. J. Phys. Chem. Solids **115**, 317–321 (2018). https://doi.org/10.1016/j.jpcs.2017.12.042
40. J. Zai, X. Qian, Three dimensional metal oxides–graphene composites and their applications in lithium ion batteries. RSC. Adv. **5**, 8814–8834 (2015). https://doi.org/10.1039/C4RA11903G
41. L. Tang, Y. Wang, Y. Li, H. Feng, J. Lu, J. Li, Preparation, structure, and electrochemical properties of reduced graphene sheet films. Adv. Funct. Mater. **19**, 2782–2789 (2009). https://doi.org/10.1002/adfm.200900377
42. M.G. Fayed, S.Y. Attia, Y.F. Barakat, E.E. El-Shereafy, M.M. Rashad, S.G. Mohamed, "Carbon and nitrogen co-doped MoS2 nanoflakes as an electrode material for lithium-ion batteries and supercapacitors" sustain. Mater. Technol. **29**, 00306 (2021). https://doi.org/10.1016/j.susmat.2021.e00306
43. J. Nie, H. Fu, Z. Li, J. Wang, S. Yao, Constructing CoFe2O4 with cubic structure by Prussian blue to provide high-performance anodes for lithium-ion batteries. Mater. Lett. **300**, 130152 (2021). https://doi.org/10.1016/j.matlet.2021.130152